Research Article

Outcomes of myocardial infarction hydrogel injection therapy in the human left ventricle dependent on injectate distribution

Renee Miller[1,+], Neil H. Davies[1], Jeroen Kortsmit[1,#], Peter Zilla[1] and Thomas Franz[1-4,*]

[1]Cardiovascular Research Unit, Chris Barnard Division of Cardiothoracic Surgery, University of Cape Town, Observatory, South Africa

[2]Programme for the Enhancement of Research Capacity (PERC), Research Office, University of Cape Town, Mowbray, South Africa

[3]Centre for Research in Computational and Applied Mechanics, University of Cape Town, Rondebosch, South Africa

[4]Centre for High Performance Computing, Rosebank, South Africa

Running title: Distribution-specific efficacy of gel injectate in infarcted human LV

+ Whitaker Fellow

[#] Claude Leon Postdoctoral Fellow

*Send correspondence to:
Dr Thomas Franz
Cardiovascular Research Unit
Faculty of Health Sciences
University of Cape Town
Private Bag X3, 7935 Observatory, South Africa
Tel: +2721406 6418, Fax: +2721 4485935
E-mail: thomas.franz@uct.ac.za

SUMMARY

Myocardial infarction therapies involving biomaterial injections have shown benefits in inhibiting progression towards heart failure. However, the underlying mechanisms remain unclear. A finite element model of the human left ventricle (LV) was developed from magnetic resonance images. An antero-apical infarct was represented at acute (AI) and fibrotic (FI) stage. Hydrogel injections in the infarct region were modelled with layered (L) and bulk (B) distribution. In the FI, injectates reduced end-systolic myofibre stresses from 291.6% to 117.6% (FI-L) and 115.3% (FI-B) of the healthy value whereas all acute infarct models exhibited sub-healthy stress levels (AI: 90.9%, AI-L: 20.9%, AI-B: 30.5%). Reduction in end-diastolic infarct stress were less pronounced for both fibrotic (FI: 294.1%, FI-L: 176.5%, FI-B: 188.2%) and acute infarct (AI: 94.1%, AI-L: 35.3%, AI-B: 41.2%). In the border zone, injectates reduced end-systolic fibre stress by 8-10% and strain from positive (AI) and zero (FI) to negative. Layered and bulk injectates increased ejection fraction by 7.4% and 8.4% in AI and 14.1% and 13.7% in FI. The layered injectate had a greater impact on infarct stress and strain at acute stage whereas the bulk injectate exhibited greater benefits at fibrotic stage. These findings were confirmed by our previous *in vivo* results.

1 INTRODUCTION

In 2002, 16.7 million people died from cardiovascular diseases worldwide, of which nearly half were attributed to coronary heart disease [1]. An estimated 80.7 million American adults (one in three) had one or more types of cardiovascular disease in 2005. Of 16 million people that suffered from coronary heart disease, about half (8.1 million) were recuperating from a myocardial infarction (MI). Up to one third of MI patients develop heart failure (HF) making MI the most common cause of HF[2].After an MI event, a process of remodelling of healthy and ischaemic tissue is initiated in an effort to restore cardiac function. The remodelling involves structural changes such as cavity dilation, hypertrophy and scar formation affecting the left ventricle (LV) [3, 4]. Although these changes occur in an attempt to maintain stroke volume (SV) and cardiac output, the LV dilation leads to an elevation of the wall stress that is postulated to be a major cause of the initial positive adaptation of the heart to turn pathological [5, 6]. Most MI therapies aim to reduce pathological remodelling that could potentially lead to HF. Substantial research has been devoted towards developing cell therapies for MI with the aim of promoting growth of new cardiomyocytes in the infarcted region. In many cell therapy approaches that rely on delivery of cells with a carrier medium, restoration or improvement of the pump function of the LV was observed [7-10]. It is, however, not well understood whether the beneficial effects of cell delivery treatments have been a result of cellular signalling, causing myocardial regeneration or decreased apoptosis, mechanical effects of increasing the infarct wall thickness due to the added carrier material or a combination of both [11].Recent research has been aimed at determining solely the mechanical effect of biological or synthetic intra-myocardial injectates on LV mechanics. Acellular biomaterial injections have been shown to reduce stresses in the infarcted ventricular wall *in vivo* [12]. Although positive results have been observed when injecting biological materials such as alginate, fibrin and decelluarised matrices, synthetic biomaterials allow for greater control of material characteristics such as elasticity and

permeability [12]. Despite positive results from *in vivo* studies, underlying mechanisms behind biomaterial injection therapy remain largely unknown.

Computational modelling has been beneficial in providing meaningful information on various cardiac pathologies including MI and HF complementary to *in vivo* research [13-20].However, only few computational studies have focussed on biomaterial injection therapies for MI. Wall et al. [21] investigated a single injection into the anterior border zone (BZ), multiple BZ injections and single injection into the infarct zone with various injection volumes and a range of mechanical properties of the injectable biomaterial. A three-dimensional finite element (FE) method for large elastic deformation of ventricular myocardium and a constitutive model representing passive and contractile anisotropic mechanical properties of healthy and impaired myocardium were implemented in a validated FE model of the LV. Material injections were represented by local adjustment of the FE mesh. Results indicated that small amounts of injected biomaterial (0.5-5% of total myocardial volume including all four chambers) reduced wall stress and improved cardiac function. This was also the first computational study to show that improvement in long-term ventricular mechanics may be achieved by passive reduction in local stress rather than adding contractile material in the infarct zone. Wenk et al. [22] computationally studied the number and placement of spherical hydrogel injections within the LV infarcted myocardium. Regular patterns of 3 x 10, 2 x1 and 3 x6 injections, respectively, were found as optimal for minimising the myofibre stress, maximising the LV stroke volume (SV) and a combination of both. In another study, Wenk et al. [23] developed two LV ovine FE models to investigate the injection of a calcium hydroxyapatite-based tissue filler in an antero-apical infarct. The injection treatment was represented as a change in stiffness of the infarcted wall and the stiffness was optimised until the infarct region was entirely akinetic. Results showed an increase in ejection fraction (EF) and a reduction in end-diastolic and end-systolic myofibre stresses in infarct and remote regions as effects of the injection treatment.

Pre-clinical *in vivo* studies [11, 24, 25] indicated that the hydrogel injectates resemble a multi-layer structure when injected during acute ischemia and a bolus when injected during the fibrotic stage of ventricular remodelling. The current study was motivated by the question of the role of these distinctly different injectate distributions on the therapeutic effects on myocardial mechanics and function of the infarcted heart which has not been addressed before. In a previous study, we investigated layered biomaterial injectates using a canine cardiac geometry [26]. In the current study, a human LV FE model was developed from MRI data. An antero-apical infarct was simulated by locally adjusting the geometry and constitutive myocardial properties of the LV. Polyethylene glycol (PEG) hydrogel injectates were represented as either multiple thin layers or a single thick layer within the infarct region and their effects investigated in an acutely and a fibrotic infarct, respectively.

2   METHODS

2.1   Finite element model generation from cardiac MRI

A cardiac magnetic resonance imaging (MRI) data set of a healthy human heart, comprising stacks of 11 cine short-axis slices (slice thickness: 7mm, slice gap: 3mm) from base to apex at 17 time points throughout one cardiac cycle, was obtained from the Department of Human Biology, University of Cape Town. At the end-systolic time point, endocardial and epicardial contours of the LV were identified using Segment 1.8 [27, 28]. Following minor manual adjustments to omit valve openings and papillary muscles, coordinate pairs (x, y) of contours, were exported for each slice. The long-axis coordinate, z, of each slice was determined from slice thickness and slice gap extracted from the MRI file header information and a scaling factor computed from Segment. The data were shifted and rotated to align the z-axis with the longitudinal axis of the LV cavity. The data were imported into Continuity 6 (National Biomedical Computation Resource, University of California, San Diego, CA, USA). Prolate-spheroidal surface meshes

were fit to the endocardial and epicardial coordinates using a least-squares method, avoiding unrealistically large curvature gradients through subsequent smoothing. A small hole was included to eliminate redundant nodes at the apex. From the endocardial and epicardial surface meshes, a three-dimensional mesh was obtained to represent the LV wall. After refining the mesh to attain six radial layers, the mesh comprised of 96 hexahedral elements described with tri-cubic Hermite basis functions in Cartesian coordinates. Nodal derivates used for interpolation were based on arc lengths. Myofibre angles [29], defined with respect to a mutually orthogonal curvilinear coordinate system, implemented throughout the LV are summarised in Table 1. Similar to the nodal coordinates, the myofibre angles were described by tri-cubic Hermite basis functions. For systolic and diastolic simulations, axisymmetric boundary conditions were applied at the epicardial basal and apical nodes. Nodal coordinates at the epicardial base as well as their circumferential and transmural derivatives were fixed. In this way, expansion of the epicardial basal contour was restricted in order to simulate the effects of stiff annuli of the valves. At the apex, nodal derivatives in the longitudinal and circumferential direction were fixed to prevent unrealistic deformations around the small apical hole [30]. Figure 1(a) illustrates the geometry and finite element mesh of the healthy LV.

2.2   Constitutive models

Passive constitutive properties of the LV myocardium was described using a transversely isotropic exponential function of Lagrangian strains that models the material as nearly incompressible [31]:

$$W = \frac{1}{2} C \left(e^{Q} - 1 \right) + C_{compr} \left(J \ln J - J + 1 \right)$$

(1)

with

$$Q = b_{ff} E_{ff}^2 + b_{xx} \left(E_{cc}^2 + E_{ss}^2 + E_{cs}^2 + E_{sc}^2 \right) + b_{fx} \left(E_{fc}^2 + E_{cf}^2 + E_{fs}^2 + E_{sf}^2 \right),$$

(2)

Where C is the stress scaling coefficient; C_{compr} is the prescribed bulk modulus; J is the determinant of the deformation gradient; b_{ff}, b_{xx} and b_{fx} are fibre strain, cross-fibre strain coefficient and shear strain coefficient; E_{ff} is fibre strain, E_{cc} is cross-fibre in-plane strain, E_{ss} is radial strain transverse to the fibre, E_{cs} is shear strain in the transverse plane, E_{fc} is shear strain in fibre – cross-fibre plane, and E_{fs} is fibre – radial coordinate plane. The second right-hand side term of the strain energy density function W represents a penalty function to model the passive myocardium as nearly incompressible [32].

Active contraction was modelled as the sum of passive stress derived from Eq. 1 and an active fibre directional stress component T_0, which is the Second Piola-Kirchhoff stress. The latter was defined by a time-varying elastance model which, between peak tension and the end of relaxation, can be described as:

$$T_0 = \frac{1}{2} T_{max} \frac{Ca_0^2}{Ca_0^2 + ECa_{50}^2} \left\{ 1 - \cos\left[\left(\frac{t - t_0}{ml_r\sqrt{2E_{11} + 1} + b} \right) \pi \right] \right\} \tag{3}$$

where m and b, are the slope and time-intercept, respectively, of the linear relaxation duration-sarcomere length relation, with $m = 1.0489$ s/μm and $b = -1.429$ s, and t_0 is the time to peak tension and T_{max} is the isometric tension achieved at the longest sarcomere length and maximum peak intracellular calcium concentration $Ca_{0,max}$ [33]. The calcium sensitivity, ECa_{50} is formulated as:

$$ECa_{50} = \frac{Ca_{0,max}}{\sqrt{\exp\left[B\left(l_r\sqrt{2E_{11} + 1} - l_0 \right) \right] - 1}} \tag{4}$$

where $B = 4.75$ μm^{-1} governs the shape of the peak isometric tension-sarcomere length relation, $Ca_{0,max}$ is the maximum peak intracellular calcium concentration, l_r is the stress-free sarcomere length, l_0 is the sarcomere length at which no tension is developed and E_{11} is fibre strain [33]. The values of the material constants for active contraction were $Ca_0 = Ca_{0,max} = 4.35$ μmol/l [34], $l_0 = 1.58$ μm [35], $l_r = 1.85$ μm and $T_{max} = 135.7$ kPa [33].

2.3 Implementation of infarcts and hydrogel injectates

A transmural infarct of 16% of the total LV wall volume was defined in an array of 24 elements (6 radial x 2 longitudinal x 2 circumferential) in the antero-apical region of the LV. To investigate the effects of MI on ventricular pump function at two time points during infarct healing, namely acute ischemia and fibrosis, the stress scaling coefficient C and infarct geometry were adjusted for the infarcted area. Cell death and degradation of structural proteins cause a decrease of the passive stiffness in the acutely infarcted myocardium [4]. Hence, the infarct stiffness was modelled as 50% ($C = 0.26$ kPa) of the healthy myocardium. As the collagen replaces the necrotic cardiomyocytes and the scar forms at the later fibrotic healing stage, the tissue stiffness increases approximately 10-fold compared to the healthy myocardium [36], represented in the models by $C = 5.2$ kPa. Non-contractility of the infarcted myocardium was implemented by setting the calcium concentration to zero in the active tension model, Eq. 3. The finite element mesh was altered to account for local wall thinning in the infarct region in the fibrotic model with an associated reduction in LV wall volume of 11.12 mL compared to the models of the healthy LV and acute infarct.

In vivo studies showed that gel injectates resemble a multi-layer, striated, structure when delivered during acute ischemia and a bolus when delivered during the fibrotic stage of infarct healing [11, 25]. Due to the striations in myocardium, the injected gel disperses in a similar pattern, aligning between myofibres [25] and spreading primarily in the longitudinal and circumferential directions. To approximate these two distinctly different distributions, the hydrogel injectates were modelled with a layered and bulk distribution, respectively. For the layered distribution, transmural element layers 2 and 5 represented hydrogel whereas layers 1, 3, 4 and 6 represented infarcted myocardium, see Figure 2. In the bulk distribution, layers 3 and 4 represented hydrogel and layers 1, 2, 5 and 6 represented infarcted myocardium. The hydrogel

was modelled as isotropic ($b_{ff} = b_{xx} = 18.5$, $b_{fx} = 1.63$), non-contractile ($Ca_0 = 0$ µmol/L) material utilising the constitutive model implemented for the myocardium. The stiffness of the hydrogel was set to 50% of the value for healthy myocardium based on experimental tests [unpublished data].

To account for the additional volume of the injectate at the acute infarct stage, the FE mesh of the acute infarct model was adjusted to locally increase the wall thickness in the infarct region. For the fibrotic infarct, the injectate-based increase in infarct wall thickness compared to the thinned infarct geometry without injectate was represented by employing the geometry of the acute infarct model. Table 2 provides cavity and wall volume for the LV, and where applicable the wall volume of the infarct region and the injectate volume for the various models. Differences in volumes between models are associated with wall thickening and thinning, and were equivalent in the corresponding models with and without injectate to ensure comparable injectate volumes.

Seven FE models were generated:

- Healthy LV (H),

- LV with acute infarct (AI),

- LV with acute infarct and layered injectate (AI-L),

- LV with acute infarct and bulk injectate (AI-B),

- LV with fibrotic infarct (FI),

- LV with fibrotic infarct and layered injectate (FI-L), and

- LV with fibrotic infarct and bulk injectate (FI-B).

2.4   Cardiac haemodynamics

Diastole was simulated by applying an increasing pressure from 0 to 1.35 kPa (10.1 mmHg) to the endocardial surface of the LV model with passive tissue properties. To calibrate the model,

the stress scaling coefficient *C* of the strain energy density function, Eq. 1, was optimised until

the end-diastolic volume (EDV) approximately matched the EDV value obtained from the MRI

dataset. The end-diastolic pressure volume relationship (EDPVR) was generated from

incremental LV pressure and volume data during diastole. Subsequently, the end-systolic

pressure volume relationship (ESPVR) was developed by adding active contraction to the

passive constitutive model. Systolic simulations were performed with a prescribed initial LV

pressure and volume. Active contraction was initiated with constant LV volume until a desired

peak pressure of approximately 13.5 kPa (100 mmHg) was reached. This simulation was

repeated twice to obtain two bracketing peak pressure values and the ESPVR determined from

the three resulting LV pressure–cavity volume pairs. The number and size of time steps for the

numerical simulations varied for each model in order to achieve convergence in minimal

computational time.

2.5   Data analysis

The functional parameters EDV, ESV (end-systolic volume), SV, EF and E_{max} were determined

from the EDPVR and ESPVR for each model. The fibre directional component of the Cauchy

stress and Green-Lagrangian strain tensors were averaged over all Gauss points for each element.

The maximum and mean fibre directional components of stress and strain were reported for the

infarct region. Mean fibre stress and strain in the infarct region and the BZ were reported as

volume-weighted mean element values according to Eq. 5 (given for strain):

$$\overline{E}_{11} = \frac{1}{n} \sum_{i=1}^{n} \left[\left(\frac{1}{m} \sum_{j=1}^{k} E_{11,j} \right) \cdot \frac{V_i}{\overline{V}} \right] \tag{5}$$

where $\overline{E}_{11}$ is the mean fibre strain, $E_{11,j}$ is the fibre strain value at Gauss point *j* of element *n, k* is

the number of Gauss points per element, V_i is the volume of element *i*, $\overline{V}$ is the mean element

volume and *n* is the number of elements in the region of interest, i.e. infarct and BZ, respectively.

3   RESULTS

3.1   Myocardial mechanics

Figure 3 illustrates end-diastolic stress and strain in myofibre directions for the infarct region and BZ of the LV for all models whereas end-systolic myofibre stress and strain measures are presented in Figure 4.

End-diastolic myofibre stress and strain

Compared to the healthy LV, the mean fibre stress in the antero-apical infarct region decreased slightly for the AI case and considerably for the AI with injectates, seeFigure 3(a). In contrast, the FI case exhibited a 2.9 fold increase in end-diastolic stress compared to the healthy case. A slightly larger stress reduction of 38.7% was indicated for the layered injectate than for the bulk injectate (35.6%) compared to the non-injected FI. However, these reduced levels remained larger than the stress reported for antero-apical region of the healthy LV. Whereas the same trends were observed for the maximum fibre stress in the infarct region (Figure 3b), the increase between healthy LV and FI (1.7 fold) and decrease between FI without and with injectate (FI-L: 28.3% and FI-B: 5.2%) were smaller. The mean end-diastolic fibre stress in the BZ increased slightly (6.2%) for the AI case but decreased by 16.9%in the FI compared to the healthy LV (Figure 3c). The reduction in BZ fibre stress in the infarct models was small for both the AI and FI cases with injected hydrogel (AI-L: 6.8%, AI-B: 4.2%, FI-L: 3.2%, FI-B: 3.4%). Supra-healthy levels of mean fibre strain were predicted in the AI region (AI: 27.2%), see Figure 3(d). Conversely, the mean infarct fibre strain was substantially lower (58.8%) in the FI case than in the same region of the healthy LV; whereas differences in the strain observed without

and with injectate were negligible. The maximum fibre strain in the infarct region (Figure 3e) showed the same trend as the mean strain: An increase for the AI case and a decrease for the FI. In the BZ, the mean fibre strain exhibited only minimal variation between the healthy, AI and FI models (Figure 3f). However, the infarct models with hydrogel injectate showed lower end-diastolic BZ fibre strain values.

End-systolic myofibre stress and strain

At the end of systole, differences in stress between the various cases were larger than at the end-diastolic time point. The mean fibre stress in the infarct region decreased by 10.0% in the AI model but increased by 191.6% in the FI case compared to the healthy LV (Figure 4a). In both the acute and fibrotic cases, the models with hydrogel injectate exhibited lower mean stress values in the infarct region than models without injectate where reductions were 74.3% (AI-L) and 66.0% (AI-B) for AI and 59.7% (FI-L) and 60.6% (FI-B) for FI. Opposite from mean stress, the maximum end-systolic fibre stress in the acutely infarcted region increased dramatically from the healthy case (Figure 4b). Maximum fibre stress in the AI decreased with inclusion of injectate. For the FI, the maximum fibre stress in the infarct region was larger than in the healthy LV with substantial stress reduction in the FI models with injectate. For the mean fibre stress in the BZ, elevated levels were reported in all infarct models compared to the healthy LV (Figure 4c) with stress values being comparable in the AI and FI models without injectate (AI 45.3% and FI 34.9%) as well as amongst the four infarct models with injectate (AI-L 31.0%, AI-B 23.4%, FI-L 33.7%, FI-B 23.5%).

The mean fibre strain in the antero-apical region was negative for the healthy LV, indicating contraction, whereas it was positive in the non-contractile antero-apical region for all infarct models, see Figure 4(d). AI and FI fibre strain increased by 107.0% and 99.3% in the BZ, respectively. Addition of injectates caused a decrease in mean fibre strain (AI-L 26.5%, AI-B 28.5%, FI-L 35.1%, FI-B 36%). Maximum end-systolic infarct fibre strain showed similar

trends. However, the injectate had a smaller effect on reducing maximum strain. In the BZ, mean fibre strain was negative in all models, although of low magnitude compared to the healthy LV, except for the AI without injectate (Figure 4f).

3.2 Cardiac haemodynamics

The EDPV and ESPV relationships are shown inFigure 5 and Figure 6, respectively. The cardiac functional parameters are summarised in Table 3. The EDV increased from 111.65 mL in the healthy LV to 113.46 mL for the AI case but decreased to 108.39 mL for the FI model. For both the acute and fibrotic cases, the models of the infarct with hydrogel injection exhibited lower EDV values than their counterpart without injectate and the healthy case. While a discernibly lower EDV was predicted for the layered gel compared to the bulk gel in the AI, the EDV was nearly the same for both gel distributions in the FI, see Table 3. SV decreased from the healthy case with 46.0 mL to the AI and FI case with 32.4 mL and 29.3 mL, respectively. The SV for each hydrogel case were comparable, only varying slightly between 32.3 mL and 32.9mL.EF in the healthy LV was 41.2% and decreased for both the AI and FI cases, to 28.5% and 27.0%, respectively. The models with hydrogel injectate exhibited improved EF of 30.6% (AI-L), 30.9% (AI-B), 30.8% (FI-L) and 30.7% (FI-B).

4 DISCUSSION

A set of FE models of a human LV was developed and employed to investigate the effects of therapeutic hydrogel injectates in the infarct region on myocardial mechanics and ventricular function. The investigations focussed on the comparison of layered and bulk distribution of the injectate at two time points after coronary occlusion namely acute ischemia and after scar formation in the fibrotic infarct. Whereas all previous computational studies on therapeutic injectates used canine [26] and ovine [21, 23] cardiac geometries, the present study employed a

human LV. The representation of layered and bulk injectate distributions were a first step to consider distinctly different distributions of biomaterials observed pre-clinically *in vivo* [11, 24, 25].

The injectates caused a marked reduction of end-systolic and end-diastolic fibre stress and strain in infarct and BZ regions. The layered hydrogel distribution had a greater impact, i.e. reduction in infarct stress and strain, at the acute stage whereas the bulk gel distribution exhibited greater benefits at the fibrotic stage. The latter agrees with our *in vivo* findings in the rat model showing significant increase in fractional shortening, as well as reduction in end-systolic diameter, for bulk hydrogel injectates compared to striated hydrogel injectates [25].Overall, the reduction in wall stress and infarct stretching facilitated through the therapeutic injectates has potential to alleviate adverse remodelling of the LV post-infarction towards heart failure.

After geometric reconstruction, there was less than 2% difference in LV wall volume and less than 1% difference in LV cavity volume between the model and MRI. Therefore, it was concluded that the final mesh accurately represented the geometry of the LV. The passive mechanics of the healthy LV model, on which all other models in this study were based, was validated by comparing LV cardiac principal strains at end-diastole to results from previous computational studies using the same transversely isotropic exponential strain energy density function. The passive material model was previously validated with experimental data [37]. The magnitude of circumferential and radial strains agreed well with results of a model by Guccione et al. modelling passive strains in a dog heart [30] with differences not exceeding 8%. Predictions of contractile mechanics, i.e. end-systolic fibre stress, were also in close agreement with predictions from computational studies using the same active stress model [30, 38, 39]. Disregarding the small stress values around the apical hole due to imposed boundary conditions, mean end-systolic healthy tissue fibre stress in the LV was 32.1kPa compared to 32.25kPa

(healthy tissue end-systolic fibre stress averaged between two models) predicted by Wenk et al. [38].

Substantially elevated myofibre stress in the infarct region was shown for the FI at both end-diastole and end-systole compared to the healthy LV. By decreasing this elevated infarct stress by up to 36%, the hydrogel injectate may contribute markedly to limiting further remodelling of the heart. Whereas the efficacy of layered and bulk injectate was very similar for mean infarct stress, the layered injectate was found to be superior with regard to reducing maximum stress both at the acute and fibrotic infarct stage.

Systolic infarct stretching, associated with wasting energy generated by healthy myocardium and reducing LV pump function [4], was indicated for both the AI and FI models. The stretching of the infarct was reduced, although not inhibited entirely, with hydrogel injectates thereby potentially recovering some systolic functionality of the LV and slowing the progression towards HF. In the acute infarct, the layered distribution appeared to be slightly more efficient than the bulk distribution.

Limited deformation of myocardium in the BZ through coupling to the infarct [4] was most apparent at end-systole with elevated mean fibre stresses and strains in the BZ of both AI and FI models compared to the healthy control. With hydrogel injectate, the end-systolic BZ fibre stresses decreased by 8-10%. End-systolic BZ fibre strain was reduced from positive (stretching) to negative (contracting) for the AI, and from zero to negative contractile in the FI case. Although stresses and strains did not return to normal levels of the healthy LV, the changes signify that hydrogel injection could help to preserve function of healthy adjacent myocardium.

The increase in wall thickness associated with the inclusion of hydrogel caused the beneficial reduction in EDV and increase in EF. This result can be attributed to the reduction in end-diastolic strain, i.e. tissue stretching, in the infarct region compared to the infarcts without injectate. Physiologically, the EDV in a FI is greater than a healthy LV due to the dilation that occurs as a result of ventricular remodelling [4, 5]. This model, however, did not account for

ventricular dilation and so does not reflect the appropriate changes in EDV as a result of a fibrotic infarct. A similar study has incorporated ventricular dilation as well as wall thinning to realistically model the post-infarct structural changes [40, 41].

EF for the healthy LV model was below the normal EF for an average human [42] and below the EF measured from MRI LV volumes. The discrepancy between modelled and physiologic EF is due to the fact that the constitutive parameters of the active tension model are based on values obtained for a canine under anaesthesia which lowers the contractility of the LV [43].As expected, the infarct models exhibited a reduction in EF compared to the healthy LV. Hydrogel injectates caused an increase in EF by 7.4% and 8.4% (layered and bulk distribution) in the AI models and by 14.1% and 13.7% in the FI models.

Although the models provide a foundation for analysis of cardiac mechanics resulting from the injection of a polymeric biomaterial, there are some limitations. In this study, the end-systolic LV configuration was used as the reference state. Since the LV is continually loaded *in vivo*, a mesh of the unloaded state is ideal for simulating diastolic filling and systolic contraction in order to approximate accurate stresses and strains at any point in the cardiac cycle. However, end-systolic [44] or mid-diastolic [45] configurations have been used previously as reference geometry since the ventricular volumes are closer to the expected unloaded diastolic volume.

Additionally, material parameters in the constitutive model were based on canine rather than human myocardium. This paper was a preliminary study where cardiac MRI of a human patient was readily available. The stress and strain results were validated against myofibre stress and strain results which used similar constitutive and active stress models. The models provide a good basis for qualitative analysis of the effect of hydrogel injectate.

Due to the geometrical adjustments of the models for wall thinning and thickening, respectively, in the infarct region, is was not possible to keep the volume of the injectate identical in the different models. However, the differences, in particular between corresponding layered and

bulk injectate representing the same infarct stage were smaller than those between the different infarct stages. Whereas effects of the volume differences cannot be excluded, it is assumed that these were secondary to the effects if the different injectate distributions.

5   CONCLUSIONS

The set of human left ventricular finite element models developed proved feasible to explore the mechanical effects involved in intra-myocardial injection therapy for myocardial infarction. The variation of the effects that different injectate distributions have at early and at late infarct stage predicted with these models agrees with our preclinical *in vivo* findings. The models can serve as a numerical framework for extended investigations of biomaterial injections for acellular treatment of myocardial infarction and potentially also as part of cell therapies.

CONFLICT OF INTEREST STATEMENT

The authors do not have conflicts of interest.

REFERENCES

1. WHO, *The atlas of heart disease and stroke*. 2008, World Health Organization: Geneva.

2. AHA, *Heart disease and stroke statistics: Our guide to current statistics and the supplement to our heart and stroke facts.* 2008, American Heart Association: Dallas.

3. Sutton MG, Sharpe N. Left ventricular remodeling after myocardial infarction: Pathophysiology and therapy. *Circulation* 2000; **101**:2981-2988.

4. Holmes JW, Borg TK, Covell JW. Structure and mechanics of healing myocardial infarcts. *Annual Review of Biomedical Engineering* 2005; **7**:223-253.

5. Opie LH, Commerford PJ, Gersh BJ, Pfeffer MA. Controversies in ventricular remodelling. *Lancet* 2006; **367**:356-367.

6. Pfeffer MA, Braunwald E. Ventricular remodeling after myocardial infarction. Experimental observations and clinical implications. *Circulation* 1990; **81**:1161-1172.

7. Kofidis T, Lebl DR, Martinez EC, Hoyt G, Tanaka M, Robbins RC. Novel injectable bioartificial tissue facilitates targeted, less invasive, large-scale tissue restoration on the beating heart after myocardial injury. *Circulation* 2005; **112**:I173-177.

8. Christman KL, Fok HH, Sievers RE, Fang Q, Lee RJ. Fibrin glue alone and skeletal myoblasts in a fibrin scaffold preserve cardiac function after myocardial infarction. *Tissue Eng* 2004; **10**:403-409.

9. Christman KL, Vardanian AJ, Fang Q, Sievers RE, Fok HH, Lee RJ. Injectable fibrin scaffold improves cell transplant survival, reduces infarct expansion, and induces neovasculature formation in ischemic myocardium. *J Am Coll Cardiol* 2004; **44**:654-660.

10. Tomita S, Mickle DA, Weisel RD, Jia ZQ, Tumiati LC, Allidina Y, Liu P, Li RK. Improved heart function with myogenesis and angiogenesis after autologous porcine

bone marrow stromal cell transplantation. *J Thorac Cardiovasc Surg* 2002; **123**:1132-1140.

11. Dobner S, Bezuidenhout D, Govender P, Zilla P, Davies N. A synthetic non-degradable polyethylene glycol hydrogel retards adverse post-infarct left ventricular remodeling. *Journal of Cardiac Failure* 2009; **15**:629-636.

12. Nelson DM, Ma Z, Fujimoto KL, Hashizume R, Wagner WR. Intra-myocardial biomaterial injection therapy in the treatment of heart failure: Materials, outcomes and challenges. *Acta biomaterialia* 2011; **7**:1-15.

13. Kerckhoffs RCP, McCulloch AD, Omens JH, Mulligan LJ. Effects of biventricular pacing and scar size in a computational model of the failing heart with left bundle branch block. *Medical Image Analysis* 2009; **13**:362-369.

14. Usyk TP, McCulloch AD. Electromechanical model of cardiac resynchronization in the dilated failing heart with left bundle branch block. *Journal of Electrocardiology* 2003; **36**:57-61.

15. Walker JC, Ratcliffe MB, Zhang P, Wallace AW, Hsu EW, Saloner DA, Guccione JM. Magnetic resonance imaging-based finite element stress analysis after linear repair of left ventricular aneurysm. *Journal of Thoracic and Cardiovascular Surgery* 2008; **135**:1094-1102.

16. Guccione JM, Salahieh A, Moonly SM, Kortsmit J, Wallace AW, Ratcliffe MB. Myosplint decreases wall stress without depressing function in the failing heart: A finite element model study. *Ann Thorac Surg* 2003; **76**:1171-1180.

17. Vetter FJ, McCulloch AD. Three-dimensional stress and strain in passive rabbit left ventricle: A model study. *Ann Biomed Eng* 2000; **28**:781-792.

18. Smith NP, Mulquiney PJ, Nash MP, Bradley CP, Nickerson DP, Hunter PJ. Mathematical modelling of the heart: Cell to organ. *Chaos, Solitons & Fractals* 2002; **13**:1613-1621.

19. Nordsletten D, McCormick M, Kilner PJ, Hunter P, Kay D, Smith NP. Fluid–solid coupling for the investigation of diastolic and systolic human left ventricular function.

International Journal for Numerical Methods in Biomedical Engineering 2011; **27**:1017-1039.

20. Niederer SA, Smith NP. At the heart of computational modelling. *Journal of Physiology* 2012; **590**:1331–1338.

21. Wall ST, Walker JC, Healy KE, Ratcliffe MB, Guccione JM. Theoretical impact of the injection of material into the myocardium - a finite element model simulation. *Circulation* 2006; **114**:2627-2635.

22. Wenk JF, Wall ST, Peterson RC, Helgerson SL, Sabbah HN, Burger M, Stander N, Ratcliffe MB, Guccione JM. A method for automatically optimizing medical devices for treating heart failure: Designing polymeric injection patterns. *Journal of Biomechanical Engineering* 2009; **131**:121011.

23. Wenk JF, Eslami P, Zhang Z, Xu C, Kuhl E, Gorman Iii JH, Robb JD, Ratcliffe MB, Gorman RC, Guccione JM. A novel method for quantifying the in-vivo mechanical effect of material injected into a myocardial infarction. *Annals of Thoracic Surgery* 2011; **92**:935-941.

24. Ifkovits JL, Tous E, Minakawa M, Morita M, Robb JD, Koomalsingh KJ, Gorman JH, Gorman RC, Burdick JA. Injectable hydrogel properties influence infarct expansion and extent of postinfarction left ventricular remodeling in an ovine model. *Proceedings of the National Academy of Sciences* 2010; **107**:11507-11512.

25. Kadner K, Dobner S, Franz T, Bezuidenhout D, Sirry MS, Zilla P, Davies NH. The beneficial effects of deferred delivery on the efficiency of hydrogel therapy post myocardial infarction. *Biomaterials* 2012; **33**:2060-2066.

26. Kortsmit J, Davies NH, Miller R, Macadangdang JR, Zilla P, Franz T. The effect of hydrogel injection on cardiac function and myocardial mechanics in a computational post-infarction model. *Computer Methods in Biomechanics and Biomedical Engineering* 2012; **epub, doi:10.1080/10255842.2012.656611**.

27. Heiberg E, Sjogren J, Ugander M, Carlsson M, Engblom H, Arheden H. Design and validation of segment - freely available software for cardiovascular image analysis. *BMC Medical Imaging* 2010; **10**:1.

28. Heiberg E, Engblom H, Engvall J, Hedström E, Ugander M, Arheden H. Semi-automatic quantification of myocardial infarction from delayed contrast enhanced magnetic resonance imaging. *Scandinavian Cardiovascular Journal* 2005; **39**:267-275.

29. Rohmer D, Sitek A, Gullberg GT. Reconstruction and visualization of fiber and laminar structure in the normal human heart from ex vivo diffusion tensor magnetic resonance imaging (dtmri) data. *Investigative Radiology* 2007; **42**:777-789.

30. Guccione JM, Costa KD, McCulloch AD. Finite element stress analysis of left ventricular mechanics in the beating dog heart. *Journal of Biomechanics* 1995; **28**:1167-1177.

31. Liu C, Hofstetter G, Mang H. 3d finite element analysis of rubber-like materials at finite strains. *Engineering Computations* 1994; **11**:111-128.

32. Doll S, Schweizerhof K. On the development of volumetric strain energy functions. *Journal of Applied Mechanics* 2000; **67**:17.

33. Guccione JM, Waldman LK, Mcculloch AD. Mechanics of active contraction in cardiac-muscle. Part 2: Cylindrical models of the systolic left-ventricle. *Journal of Biomechanical Engineering* 1993; **115**:82-90.

34. Ter Keurs H, *Calcium and contractility*, in *Cardiac metabolism*, Drake-Holland, A J, Editor. 1983, Wiley: New York. p. 73-99.

35. Ter Keurs H, Rijnsburger W, Van Heuningen R, Nagelsmit M. Tension development and sarcomere length in rat cardiac trabeculae. Evidence of length-dependent activation. *Circulation Research* 1980; **46**:703.

36. Sun K, Stander N, Jhun C, Zhang Z, Suzuki T, Wang G, Saeed M, Wallace A, Tseng E, Baker A. A computationally efficient formal optimization of regional myocardial contractility in a sheep with left ventricular aneurysm. *Journal of biomechanical engineering* 2009; **131**:111001.

37. Omens J, May K, McCulloch A. Transmural distribution of three-dimensional strain in the isolated arrested canine left ventricle. *American Journal of Physiology- Heart and Circulatory Physiology* 1991; **261**:H918.

38. Wenk JF, Eslami P, Zhang Z, Xu C, Kuhl E, Gorman Iii JH, Robb JD, Ratcliffe MB, Gorman RC, Guccione JM. A novel method for quantifying the in-vivo mechanical effect

of material injected into a myocardial infarction. *The Annals of Thoracic Surgery* 2011; **92**:935-941.

39.   Walker JC, Ratcliffe MB, Zhang P, Wallace AW, Fata B, Hsu EW, Saloner D, Guccione JM. Mri-based finite-element analysis of left ventricular aneurysm. *Am J Physiol Heart Circ Physiol* 2005; **289**:H692-700.

40.   Kortsmit J, Davies NH, Miller R, Zilla P, Franz T. Computational predictions of improved wall mechanics and function of the infarcted left ventricle at early and late remodeling stages: Comparison of layered and bulk hydrogel injectates. *Journal of Biomechanical Engineering* 2012; **in review**.

41.   Kortsmit J, Davies NH, Miller R, Zilla P, Franz T. The mechanical effects of layered and bulk hydrogel injectates in the cardiac left ventricle at early and late post-infarction stages: A computational study. *Journal of Cardiac Failure* 2012.

42.   Schlosser T, Pagonidis K, Herborn CU, Hunold P, Waltering K-U, Lauenstein TC, Barkhausen J. Assessment of left ventricular parameters using 16-mdct and new software for endocardial and epicardial border delineation. *American Journal of Roentgenology* 2005; **184**:765-773.

43.   Guccione JM, McCulloch AD. Mechanics of active contraction in cardiac muscle. Part 1: Constitutive relations for fiber stress that describe deactivation. *J Biomech Eng* 1993; **115**:72-81.

44.   Walker JC, Ratcliffe MB, Zhang P, Wallace AW, Fata B, Hsu EW, Saloner D, Guccione JM. Mri-based finite-element analysis of left ventricular aneurysm. *American Journal of Physiology - Heart and Circulatory Physiology* 2005; **289**:H692-H700.

45.   Sermesant M, Razavi R, *Personalized computational models of the heart for cardiac resynchronization therapy*, in *Patient-specific modeling of the cardiovascular system*, Kerckhoffs, R C P, Editor. 2010, Springer: New York. p. 167-182.

Tables

Table 1. LV myofibre angles applied to various locations of the reconstructed LV geometry [29]

Radial Location	Longitudinal Location		
	Basal	Equatorial	Apical
Epicardial	-30.45°	-28.16°	-25.88°
Midwall	9.55°	10.11°	10.67°
Endocardial	49.55°	48.38°	47.21°

Table 2. LV cavity volume, wall volume of LV and infarct region and volume of the injectate for the different models

Model	Volume			
	LV cavity (mL)	LV wall (mL)	Infarcted wall (mL)	Injectate (mL)
Healthy (H)	53.4	129.3	-	-
Acute Infarct (AI)	53.4	129.3	20.6	-
Acute Infarct + Layered Gel (AI-L)	50.1	137.5	18.4	9.0
Acute Infarct + Bulk Gel (AI-B)	50.1	137.5	19.2	8.2
Fibrotic Infarct (FI)	55.9	118.2	13.8	-
Fibrotic Infarct + Layered Gel (FI-L)	53.4	129.3	13.7	6.9
Fibrotic Infarct + Bulk Gel (FI-B)	53.4	129.3	13.8	6.8

Table 3. Cardiac functional parameters for all models: End-diastolic volume (EDV), end-systolic volume (ESV), stroke volume (SV) and ejection fraction (EF)

Model	EDV (mL)	ESV (mL)	SV (mL)	EF (%)
Healthy (H)	111.7	65.6	46.0	41.2
Acute Infarct (AI)	113.5	81.1	32.4	28.5
Acute Infarct + Layered Gel (AI-L)	105.8	73.5	32.3	30.6
Acute Infarct + Bulk Gel (AI-B)	106.6	73.7	32.9	30.9
Fibrotic Infarct (FI)	108.4	79.1	29.3	27.0
Fibrotic Infarct + Layered Gel (FI-L)	105.6	73.1	32.5	30.8
Fibrotic Infarct + Bulk Gel (FI-B)	105.7	73.2	32.4	30.7

Figures
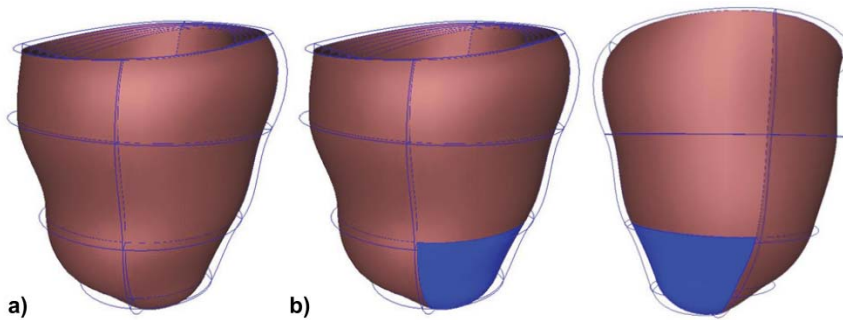
Figure 1. Geometry and finite element mesh of the non-infarcted LV (a) and two different views of LV with antero-apical infarct (b).
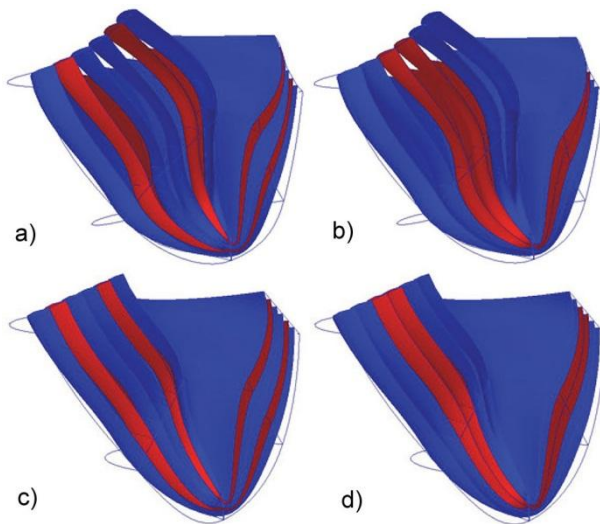
Figure 2. Cross-sectional apical view of infarcted region with different injectate distributions: a) Layered gel injectate in AI represented as transmural layers 2 and 5,b) Bulk injectate in AI represented as transmural layers 3 and 4, c) Layered injectate in FI represented as transmural layers 2 and 5, and d) Bulk injectate in FI represented as transmural layers 3 and 4.
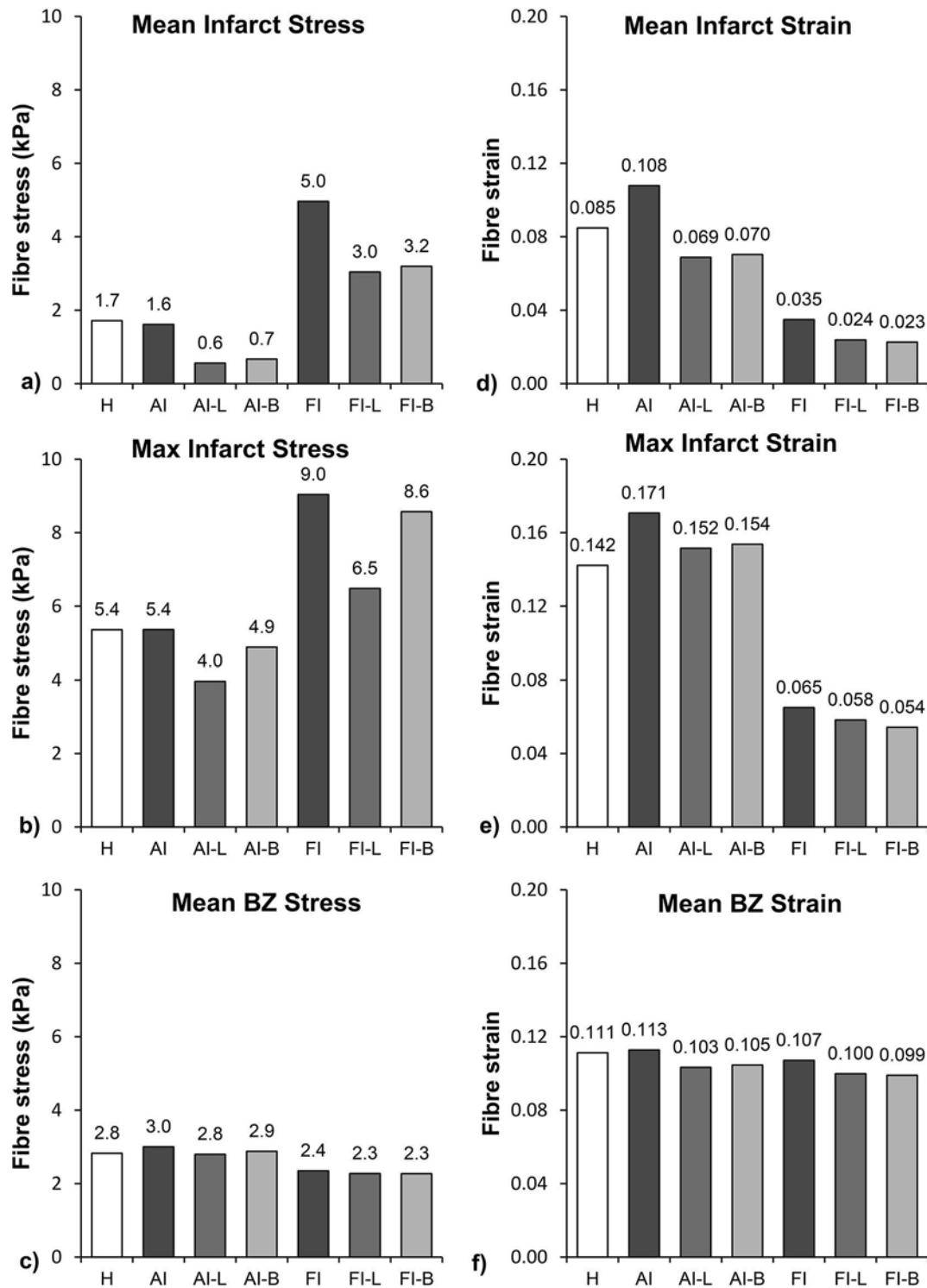
Figure 3. End-diastolic myofibre stresses and strains: a) Mean stress in the region of the infarct, b) maximum stress in the region of the infarct, c) mean stress in the border zone, d) mean strain in the region of the infarct, e) maximum strain in the region of the infarct, and f) mean strain in the border zone.
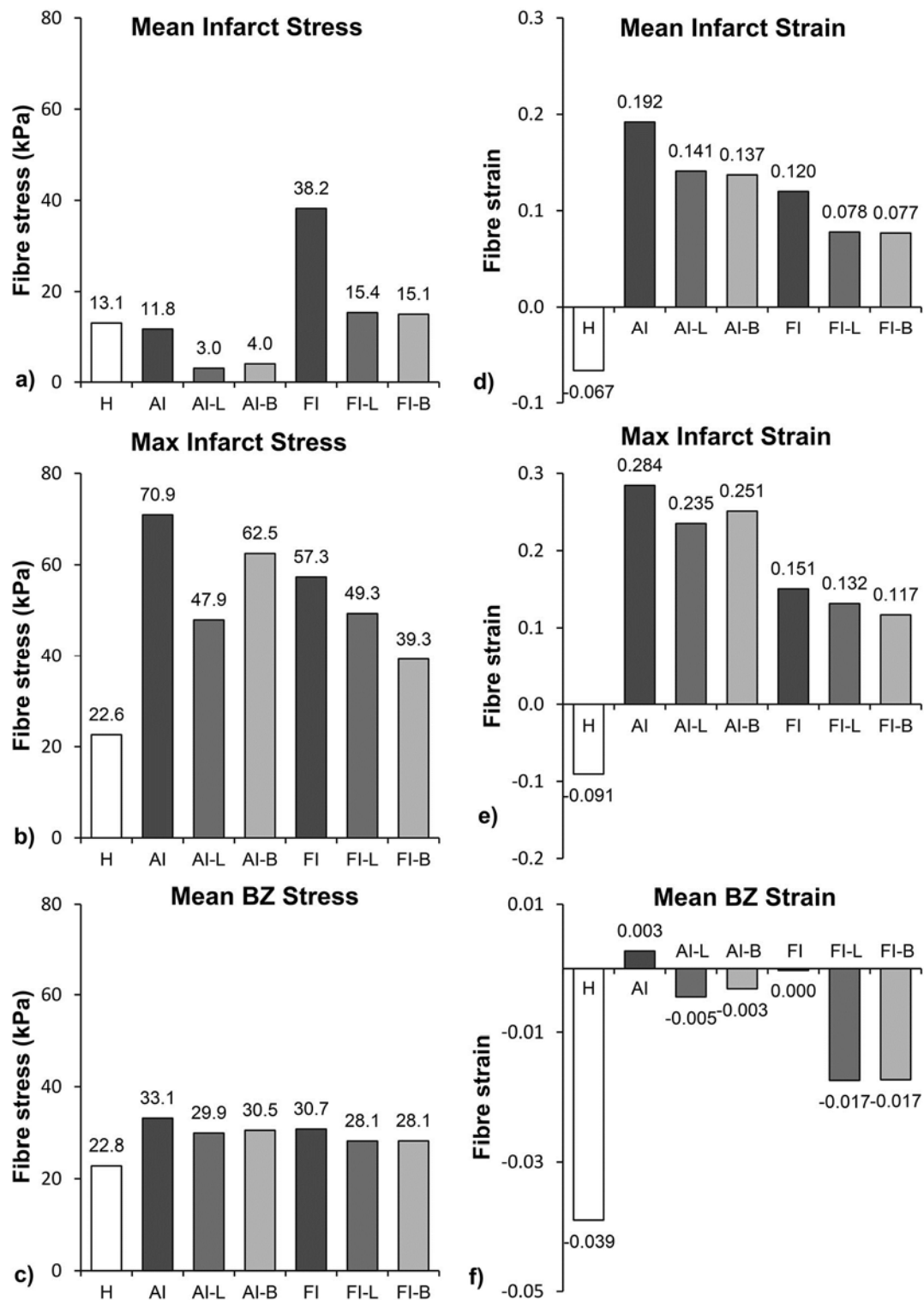
Figure 4. End-systolic myofibre stresses and strains: a) Mean stress in the region of the infarct, b) maximum stress in the region of the infarct, c) mean stress in the border zone, d) mean strain in the region of the infarct, e) maximum strain in the region of the infarct, and f) mean strain in the border zone.
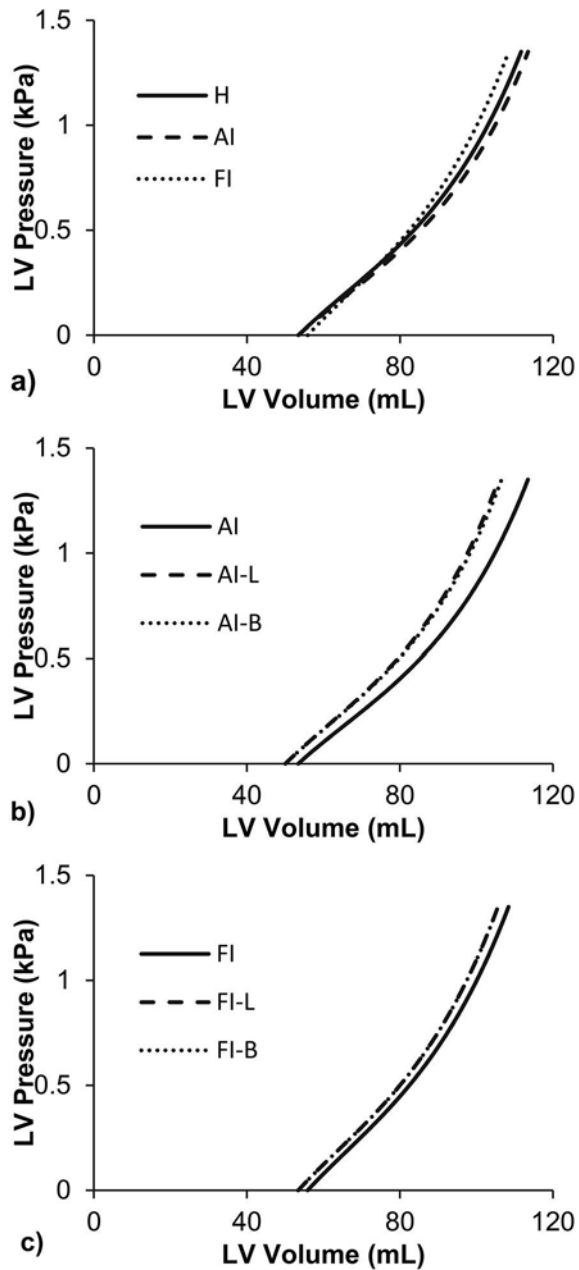
Figure 5. Comparison of end-diastolic pressure-volume relationships for: a) Healthy LV and LV with acute and fibrotic infarcts, b) LV with acute infarct without injectate, with layered injectate and with bulk injectate, and c) LV with fibrotic infarct without injectate, with layered injectate and with bulk injectate. (Note: In diagram c, the EDPVR for FI-L and FI-B are nearly identical and the two curves coincide.)
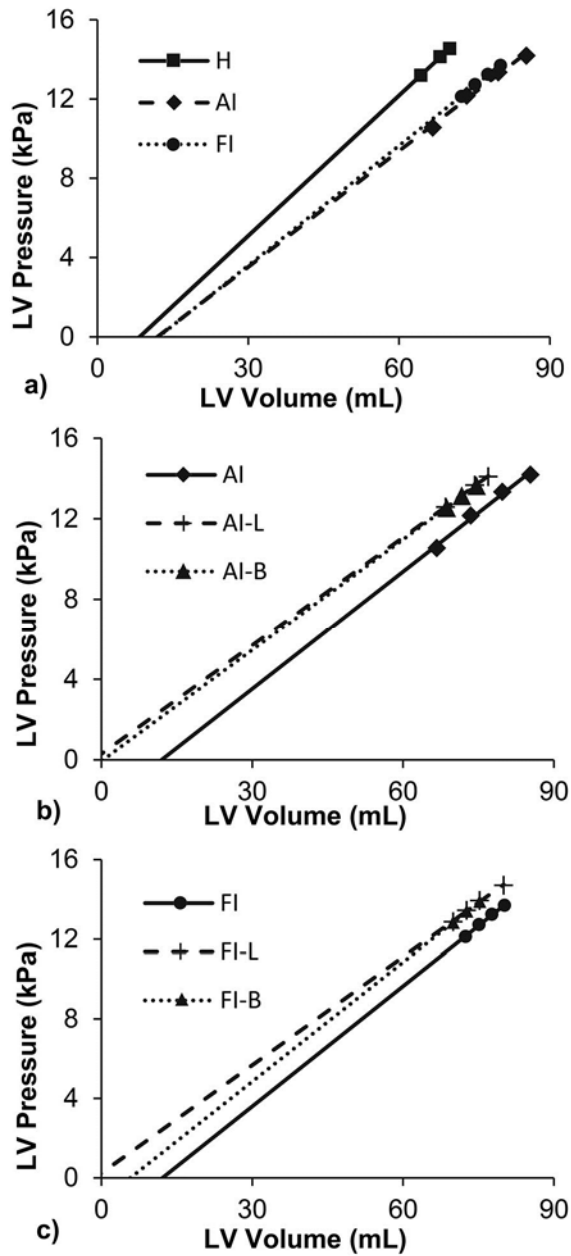
Figure 6. Comparison of end-systolic pressure-volume relationships for: a) Healthy LV and LV with acute and fibrotic infarcts, b) LV with acute infarct without injectate, with layered injectate and with bulk injectate and c) LV with fibrotic infarct without injectate, with layered injectate and with bulk injectate.